

# A series of avoided crossings of resonances in the system of several different dielectric resonators results in giant $Q$ -factors

K. Pichugin, A. Sadreev, and E. Bulgakov

Kirensky Institute of Physics, Federal Research Center KSC SB RAS, 660036, Krasnoyarsk, Russia

(\*Electronic mail: almas@tnp.krasn.ru)

(Dated: 13 July 2023)

We perform optimization of  $Q$ -factor in the system of freestanding three/four/five/six coaxial subwavelength dielectric disks over all scales. Each parameter contributes almost one order of magnitude of the  $Q$ -factor due to multiple avoided crossings of resonances to give totally the unprecedented values for the  $Q$ -factors:  $6.6 \cdot 10^4$  for the three,  $4.8 \cdot 10^6$  for four,  $8.5 \cdot 10^7$  for five and one billion for six freestanding silicon disks. By multipole analysis of the resulting hybridized resonant mode we observe that such extremely large values of the  $Q$ -factor are attributed to strong redistribution of radiation that originates from almost exact destructive interference of dominating complex multipole radiation amplitudes.

## I. INTRODUCTION

Since the famous paper by Gustav Mie<sup>1</sup>, the engineering of dielectric cavities in optics and photonics has been a long-standing area for the application of various ideas and approaches to enhance the quality factor  $Q$  due to its paramount importance in both applied and fundamental research. However there is a fundamental upper limit for  $Q$ -factor because of leakage of radiation power from isolated dielectric resonator into the radiation continuum<sup>2,3</sup>. There are many ways to enormously boost  $Q$ -factor. For example, one can use Fabry-Pérot resonances or hide a cavity in photonic crystals (PhC)<sup>4-7</sup>. Whispering gallery modes (WGM) in the cavities with convex smooth boundaries such as cylindrical, spherical or elliptical cavities also show giant magnitudes of  $Q$ -factor<sup>8-12</sup>.

Cardinally different way is bound states in the continuum (BICs), which provide unique opportunity to confine and manipulate electromagnetic wave within the radiation continuum (see reviews<sup>13-18</sup>). The phenomenon of BICs is based on that electromagnetic power can leak only in selected directions given by diffraction orders, if to arrange dielectric cavities into a periodical array<sup>19-21</sup>. Although in reality the number of cavities  $N$  in an array cannot be infinite, the  $Q$ -factor grows fast with  $N$ : quadratically for symmetry protected (SP) quasi-BICs<sup>22-24</sup> or cubically for accidental BICs<sup>23,25,26</sup>. However this way of engineering of quasi-BICs goes away the dielectric structures (DS) from compactness. For example, to achieve  $Q$ -factor of the order  $10^5$ , we need at least several tens of silicon disks<sup>24,27,28</sup> or silicon cuboids<sup>29</sup>. The best results for the  $Q$ -factor were reported by Taghizadeh and Chung<sup>22</sup> with  $Q \sim 10^5$  for 10 long identical silicon rods. In general, all the ways to achieve the extremely high  $Q$ -factor listed above require an extended DS in which the mode volume grows too<sup>7,30</sup>.

In the present paper we show that this way of boosting the  $Q$ -factor by a periodical array of  $N$  identical resonators is not optimal. We consider a system of only a few resonators each of different scales variation of which causes a cascade of ACRs to radically boost  $Q$ -factor. As a result, we have achieved giant magnitudes of  $Q$ -factor considerably exceed-

ing the results for quasi-BICs maintaining nearly the same mode volume (see Table I). ACR<sup>31,32</sup> is a general and fundamental phenomenon that describes the behavior of eigenfrequencies of an open resonator, which are complex due to coupling with the radiation continuum. Whether the resonant frequencies exhibit either crossing or anticrossing depends on the mechanism of interaction<sup>32-34</sup>. In any case, two resonances near ACR interfere in constructive and destructive ways. The latter way enhances  $Q$ -factor and has been successfully used in many types of single resonators<sup>35-37</sup>. As a result the  $Q$ -factor can be strongly enhanced as has been demonstrated for different choices of dielectric resonators<sup>35,37-44</sup>. Example of such a super cavity mode due to hybridization of resonances is highlighted by yellow open circle in Fig. 1 (a) for the case of disk shaped resonator. In a single silicon disk with permittivity  $\epsilon = 12$  the  $Q$ -factor reaches  $Q = 150$  for  $h_1/r = 1.4157$  as Fig. 1 (b) shows. Along with that the

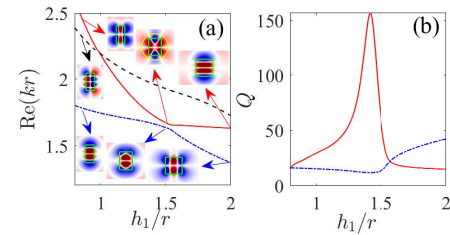


FIG. 1. (a) ACR of the two resonant even modes of a single silicon disk with  $\epsilon = 12$  shown by red solid line and blue dash-dot line for variation of aspect ratio<sup>39</sup>. The insets show hybridization of modes (the tangential component of electric field  $E_\phi$  of TE modes). Black dash line shows the evolution of the odd resonant mode, which is decoupled from former modes. (b) Respective considerable enhancement of the  $Q$ -factor due to ACR.

ACR approach to enhance the  $Q$ -factor has been developed for a system of photonic molecules owing to coupling between resonators<sup>12,38,45-52</sup>.

## II. THE PROBLEM STATEMENT

Recently we have developed a way to enhance the  $Q$ -factor by extending the number of resonators in photonic molecule spaced at different distances on the example of three and four coaxial silicon disks<sup>53</sup>. As a result we achieved  $Q \approx 10^6$  for four disks of identical radii. In the present paper we put forward a novel strategy of cascading ACRs in a system of  $N$  disks in order to achieve unprecedented magnitudes of  $Q$ -factor. We consider disks to be freestanding and coaxial, made of silicon with permittivity  $\epsilon = 12$  for wavelength  $\lambda \approx 1.55\mu\text{m}$  at which material losses are negligible<sup>54</sup>. The eigenmodes of the system are classified according to irreducible one-dimensional representations of rotations around the symmetry axis specified by the azimuthal index  $m$ . We will focus on the case  $m = 0$  since the solutions of Maxwell equations are additionally split by polarization that also simplifies the problem. A system of  $N$  coaxial disks offers  $3N - 1$  scales to vary in general:  $N$  radii  $r_j$ ,  $N$  heights  $h_j$ ,  $j = 1, 2, \dots, N$ , and  $N - 1$  distances  $L_{12}, L_{23}, \dots, L_{N-1N}$ . Considering that one of the scales should be chosen for dimensionless ratios, we obtain a total of  $3N - 2$  parameters. Optimization over this number of parameters even for a small number of resonators is an extremely time-consuming computational problem. It is reasonable to choose systems that are symmetric with respect to the inversion of the axis of rotational symmetry, which radiates less compared to non-symmetric designs. Guiding by this assumption,  $N_p = \text{fix}((3N - 1)/2)$  scale parameters are left to vary, where a term 'fix' means a rounding to the nearest integers towards zero. Particular cases of the systems with  $N = 3, 4, 5, 6$  are shown in Fig. 2.

Our central approach is based on dividing the system into two subsystems: an internal subsystem of  $N - 2$  disks and an external dimer represented by the first and the last disks. Assume, the first inner subsystem has already been optimized to find the hybridized resonant mode  $\psi_{N-2}$  with maximal  $Q$ -factor. This mode could be even or odd with respect to the axis inversion. The outer dimer provides the resonant modes  $\psi_2$  of the same symmetry. For variation of scales of the dimer, we have multiple ACRs of it's resonances with the optimized resonance of the internal subsystem. As a result we obtain a hybridized resonant mode  $\psi_N$  with enhanced  $Q$ -factor of the total system. However it must not be supposed that the solution of the problem is finished. The interaction of two subsystems slightly perturbs the optimized mode  $\psi_{N-2}$ , which obliges fine-tuning of the inner subsystem. Therefore, we must continue the process of successive optimizations.

Technically the strategy looks as follows. To enhance  $Q$ -factor we perform an optimization procedure in parametric space for initial sets of parameters. Each initial set lead to a local maximum of the  $Q$ -factor. It is reasonable to fix at first the scale parameters for inner subsystem of  $N - 2$  disks tuned to have maximal  $Q$ -factor while the 3 remaining scales  $L_{12}, r_1, h_1$  of outer dimer evolve in a three-dimensional parametric space. In view of time consuming calculations we apply the Nelder-Mead simplex optimization method for  $Q$ -factor in total  $N_p$ -dimensional parametric space. As a result, we achieved giant magnitudes of the  $Q$ -factor  $6.6 \cdot 10^4$  for three,  $8.5 \cdot 10^7$  for

five silicon disks at frequency  $kr \approx 1.75$  and  $4.8 \cdot 10^6$  for four,  $1.3 \cdot 10^9$  for six silicon disks at frequency  $kr \approx 2.2$  maintaining nearly the same mode volume (see Table I).

## III. A CASCADE OF AVOIDED CROSSINGS OF RESONANCES IN THE SYSTEM OF SEVERAL COAXIAL DISKS

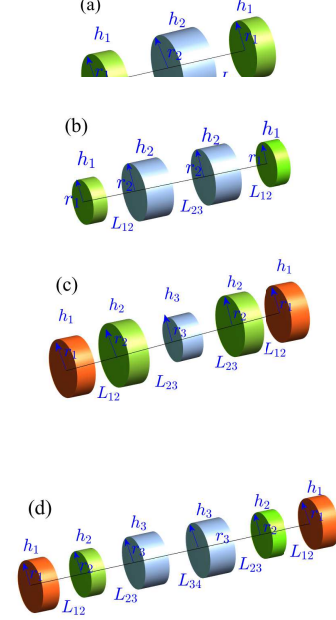


FIG. 2. (a) Disk inside dimer. (b) Dimer inside dimer. (c) System (a) inside dimer. (d) System (b) inside dimer. All freestanding disks with  $\epsilon = 12$  are coaxial but have different radii and heights to form symmetric structure. Radius of the middle gray disk(s) is used as scale  $r$  in the systems. We assume azimuthal number  $m = 0$  unless otherwise noted.

### A. Three disks

To illustrate the strategy for achieving maximal  $Q$ -factor outlined in section II we consider at first the system of 3 disks sketched in Fig. 2 (a) with 4 independent parameters  $r_1, L_{12}, h_1, h_2$  referred to the radius  $r$  of central disk. First, we place already optimized one disk  $h_2/r = 1.4157$  (see mode 1 in Table I) between 2 disks with the same aspect ratio and vary distance  $L_{12}$  only. At large distance  $L_{12}/r$  the resonances are almost degenerate and marked by 'x' in Fig. 3 (a). Drawing closer, the disks interact according to the law  $e^{ikL_{12}}/L_{12}^2$ <sup>55</sup> because of radiation of leaky resonant modes by one disk and subsequent scattering by the others. Couplings between these supercavity modes splits them into three modes with spiral behavior shown in Fig. 3 (a) with three  $Q$ -factor peaks at corresponding distances as plotted in Fig. 3 (b). Insets show field configurations of disks related to these  $Q$ -factor peaks. As a

result, we obtain a total gain in  $Q$ -factor 4 times more than for the case of the single disk marked by red cross in Fig. 3 (b).

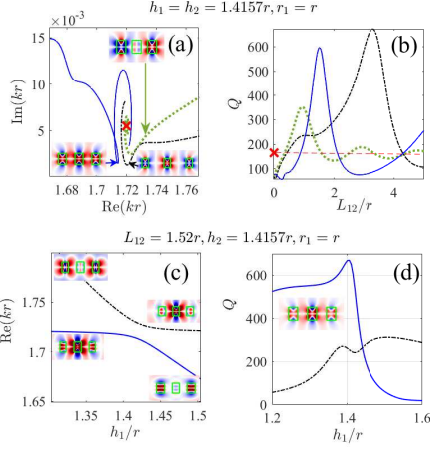


FIG. 3. (a) The first step of optimization over distance  $L_{12}$  between 3 identical disks with fixed parameters  $h_1 = h_2 = 1.4153r$ ,  $r_1 = r$ . Corresponding dependence of the  $Q$ -factor (b). The  $Q$ -factor reaches maxima at  $L_{12} = 0.945r$ ;  $Q = 350$  for green line (mode profile  $\text{Re}(E_\phi)$  is shown on the middle inset of (a)),  $L_{12} = 1.525r$ ;  $Q = 600$  for blue line and (mode profile is shown on the left inset of (a)),  $L_{12} = 3.29r$ ;  $Q = 670$  for black line (mode profile is shown on the right inset of (a)). (c) The second step of optimization over  $h_1/r$  with fixed  $L_{12} = 1.52r$ ,  $h_2 = 1.4157r$ ,  $r_1 = r$ . The  $Q$ -factor (d) reaches maximum at  $h_1 = 1.4031r$ ;  $Q = 670$ .

In the next step of the optimization method, we fix  $L_{12}/r = 1.52$  at which we get maximum value of  $Q = 600$  and vary the height of outer disks  $h_1$ . This variation gives the ACR of Fabry-Pérot-like mode, which depends strongly on  $h_1$ , and Mie-like mode, which depends weakly on  $h_1$ . This phenomenon, illustrated in Fig. 3 (c), leads to a further enhancement of the  $Q$ -factor up to  $Q = 670$  as shown in Fig. 3 (d).

At the third step, we allow the radius  $r_1$  of the outer disks to vary, while all other parameters are fixed to match the maximum  $Q$ -factor in the second step. In contrast to the previous case, the Mie-like resonant mode of outer disks is strongly dependent on  $r_1$ , while the Fabry-Pérot-like mode is weakly dependent on  $r_1$ . A selected event of ACRs of these modes is shown in Fig. 4 (a), which again raises the  $Q$ -factor up to 800.

Variation of height of the inner disk  $h_2$  while all other parameters are fixed for  $Q = 800$  closes the first round optimization procedure in full four-dimensional parametric space. The fourth step shown in Fig. 4 (c) boosts the  $Q$ -factor twice compared to the previous step, as seen from Fig. 4 (d). Repeating these rounds, at the end of the optimization procedure we obtain  $Q = 6.6 \cdot 10^4$  (see the mode 4 in Table I).

Another way to shed light on the enormous enhancement of the  $Q$ -factor is to see the evolution of resonances along the trajectory obtained by the traditional gradient descent method. This method give us point  $\mathbf{X}_\infty$  in a parametric space with local

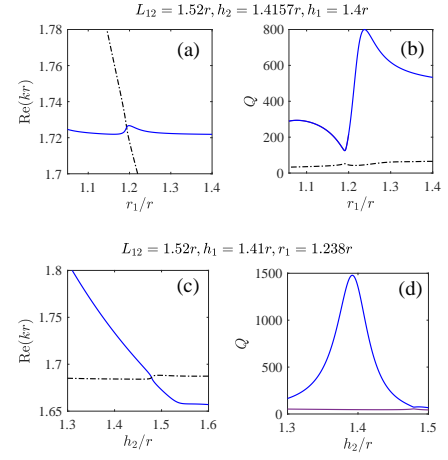


FIG. 4. Consequent ACRs over variation of different scales in the system of three disks.

maximum of  $Q$ -factor, which are the limit point of iterations

$$\mathbf{X}_{n+1} = \mathbf{X}_n + \eta \nabla Q(\mathbf{X}_n), n \rightarrow \infty \quad (1)$$

with appropriately chosen step  $\eta$ .

The total result of the method can be represented as a trajectory in the four-dimensional parametric space, whose length is determined as a curvilinear integral

$$S = \int_{\mathbf{X}_0}^{\mathbf{X}_\infty} \nabla F ds, \quad (2)$$

where

$$F = \frac{1}{r} \sqrt{h_1^2 + h_2^2 + L_{12}^2 + r_1^2} \quad (3)$$

and  $\mathbf{X}_0$  is an initial point of evolution. The evolution of the three relevant complex eigenfrequencies of the three-disk system is presented in Fig. 5 as a function of length  $S$ . In Fig. 5 we can see typical ACR-like behavior: the real parts of the green and blue lines cross (Fig. 5 (b)) while the imaginary parts repel each other (Fig. 5 (c)). The interaction of at least 3 eigenfrequencies results in enormous enhancement of the  $Q$ -factor on the red line.

There are a few points in the full four-dimensional parametric space to which the optimization method converges. In this section, we present only the most outstanding results, which exceeds values of the first iteration shown in Fig. 4 by several orders of magnitude. Among the local maxima of the  $Q$ -factor there are eigenfrequencies with unprecedented  $Q = 5.8 \cdot 10^4$  and  $Q = 6.6 \cdot 10^4$ , as shown in Fig. 6. In both cases, we have very similar supercavity modes in the middle disk while the structure of EM field in the outer dimer is different. It is worth noting that optimized mode for 5 disks (mode 5 in Table I) is somewhat combination of the above modes: EM field in disk 1 looks like EM field in disk 1 of mode 4 while EM field in disk 2 looks like EM field in disk 1 of mode 3 in Table I. Thus, we can conclude that the outer dimer plays an important role in resonant shielding of the supercavity mode radiation.

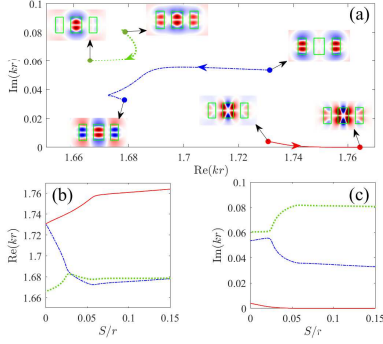


FIG. 5. (a) Evolution (1) of complex eigenfrequencies in the four-dimensional parametric space of all scales in a system of three coaxial disks.  $\mathbf{X}_0$  is given by  $r_1 = r, h_1 = r, L_{12} = 0.945r, h = 1.4157r$ . The final point  $\mathbf{X}_\infty$  correspond to the mode 4 in Table I.

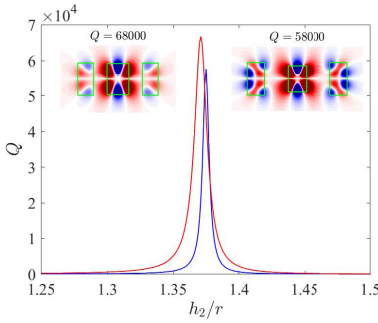


FIG. 6. Dependence of the  $Q$ -factor on  $h_2/r$  for optimized modes 3 (blue) and 4 (red) in Table I.

Because of the even symmetry of the supercavity mode, there are no ACR of this mode with resonant odd dimer modes.

Next, let us consider the four coaxial disks sketched in Fig. 2 (b). By virtue of inversion symmetry, we represent the system in the form of two dimers: internal and external. In total, we have five scale parameters for ACRs: two heights  $h_1$  and  $h_2$ , the two lengths of the dimers expressed via the two distances  $L_{12}$  and  $L_{23}$ , and, finally, the radius  $r_1$  of the outer dimer. All parameters are considered in respect to the radius of the inner dimer  $r$ . We omit the iteration steps for all five parameters of the system of two dimers. In addition, the reader can find some scenarios for ACRs for variation of four scales: two heights and two distances for identical radii  $r_1 = r$  in our previous publication<sup>53</sup>. This allows to boost the  $Q$ -factor up to one million (see mode 7 in Table I). In the present paper, we perform the final step by optimizing all 5 parameters.

Similar to the case of three disks, shown in Fig. 3, we have a Mie-like mode of the outer dimer, labelled as 1 in Fig. 7 (a), which strongly depend on the radius  $r_1$  of external dimer. The other two Fabry-Pérot-like modes, labelled as 2 and 3, are mostly localized in the inner dimer have weak dependence on  $r_1$ . As a result, we observe a cascade of ACRs around  $r_1/r = 0.8$ , highlighted by yellow open circles, which, however, do not lead to magnificent enhancement of  $Q$ -factor. In contrast to these conventional ACRs, we observe a slightly no-

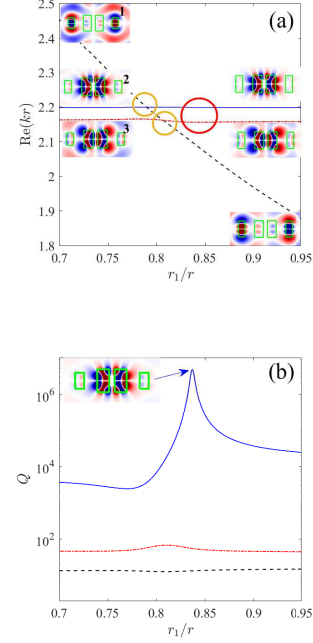


FIG. 7. (a) The final step of ACR for variation of radius  $r_1$  of external dimer relative to the radius of internal dimer  $r$  with strong enhancement of the  $Q$ -factor (b).

ticeable ACR around  $r_1/r = 0.85$  with the Fabry-Pérot-type-like modes of outer dimer. This results in a giant boosting of  $Q$ -factor up to almost five millions, and can be explained by a cumulative effect of the interaction of nearby resonances.

In Table I we collect the final configurations of systems of five and six freestanding coaxial silicon disks after the optimization procedure in parametric spaces of dimensions 7 and 8, respectively. It can be seen that the outer dimer almost completely shields radiation from the inner subsystem due to the ACR of Fabry-Pérot-like resonant mode of external dimer with resonant mode of internal subsystem, which has been already optimized for the maximum  $Q$ -factor. These cases show more impressive  $Q$ -factor results about  $5.8 \cdot 10^7$  and one billion (see Table I). Similar results can be achieved by employing WGM modes in resonators or periodical quasi-BICs, however, at the cost of increasing the radius or number of identical resonators. This, in turn, increases mode volume.

#### IV. MULTIPOLE RADIATION FOR AVOIDED CROSSING OF RESONANCES

There is a useful tool to understand the nature of the extremely high quality factor through multipole decompositions<sup>56</sup>. This tool sheds light on the origin of high  $Q$ -factor in the isolated disk<sup>41,57</sup> and the origin of bound states in the continuum<sup>53,58</sup>. In far field region, EM field can



be expanded as

$$\mathbf{E}(\mathbf{x}) = \sum_{l=1}^{\infty} \sum_{m=-l}^l [a_{lm} \mathbf{M}_{lm}(\mathbf{x}) + b_{lm} \mathbf{N}_{lm}(\mathbf{x})], \quad (4)$$

where  $\vec{M}_l^m$  and  $\vec{N}_l^m = \frac{1}{k} \nabla \times \vec{M}_l^m$  are the vector spherical harmonics<sup>59,60</sup>. Then the relative radiated power of each electric and magnetic multipole of order  $l$  is determined by the squares of the decomposition amplitudes<sup>56</sup>

$$P_{l0} = P_{l0}^{TE} + P_{l0}^{TM} = P_0^{-1} [|a_{l0}|^2 + |b_{l0}|^2] \quad (5)$$

where  $P_0$  is the total power radiating through the sphere with large radius  $P_0 = \sum_{l=1}^{\infty} [|a_{l0}|^2 + |b_{l0}|^2]$ . For the present case of coaxial disks with inversion symmetry and azimuthal number  $m = 0$ , the decomposition (4) is substantially reduced to have an even  $l$  for the symmetric solutions shown in Fig. 6, and odd  $l$  for the antisymmetric solutions shown in Fig. 7<sup>61</sup>.

The extreme  $Q$ -factor is associated with a strong redistribution of multipole radiation towards high-order multipoles, because of almost exact total destructive interference of low-order multipole amplitudes. Using the formalism described in Ref.<sup>62</sup> (Eq. (1.69)), we separate contributions from subsystems assembling the DS in the far field region. For the case of three disks, we distinguish multipole radiation from the inner disk and outer dimer, whose complex amplitudes  $a_{l0}$  in the series Eq. (4) are presented in Fig. 8. On subplots (a) and

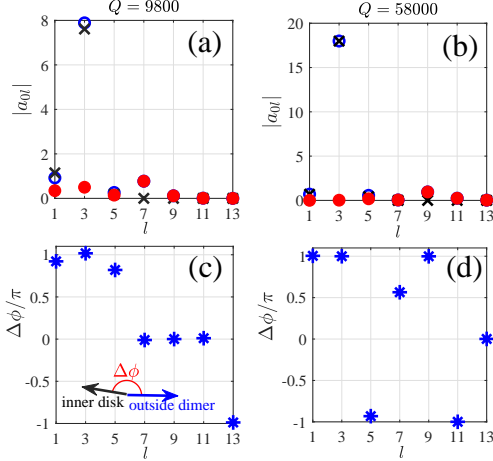


FIG. 8. The multipole radiation amplitudes  $a_{l0}, l = 1, 3, 5, \dots$  in Eq. (4) from the system of three disks of identical radii (mode 2 in Table I,  $Q = 9.8 \cdot 10^3$ ) (a), (c) and of different radii (b), (d) (mode 3 in Table I,  $Q = 5.8 \cdot 10^4$ ). The amplitudes of inner/outer dimer disk marked by crosses/open circles and amplitudes of the total system of three disks are marked by red closed circles.

(b), the markers 'o' and 'x' correspond to amplitudes  $|a_{l0}|$  of the multipole radiation from the subsystems of the inner disk and outer dimer, respectively, while the red closed circles show the multipole coefficients of the total DS, normalized by  $P_0 = \sum_l |a_{l0}|^2 = 1$ . Subplots (c) and (d) show the phase difference between the complex amplitudes of the multipole radiation of the subsystems: the inner disk and outer dimer. Left panels of Fig. 8 show the case of maximum  $Q$ -factor

$9.8 \cdot 10^3$  achieved by ACR when optimizing 3 parameters  $h_1, h_2$  and  $L_{12}$  with  $r_1 = r$ . One can see strong multipole radiation for  $l = 3$  from both inner disk and outer disks. However, these complex amplitudes  $a_{30}$  from both part, sketched by arrows in the complex plane, have almost the same moduli  $|a_{30}|$  and a phase difference close to  $180^\circ$ , which results in nearly full destructive interference of multipole radiation at  $l = 3$ . The total multipole radiation of the DS for  $l = 3$  vanishes as shown by red closed circle in Fig. 8 (a). Note that there is still small multipole radiation at  $l = 7$  from the outer dimer, while the radiation from the inner disk is mostly suppressed.

Now let us consider the right panels of Fig. 8, which show multipole radiation with  $Q = 5.8 \cdot 10^4$  achieved by optimizing all possible parameters  $h_1, r_1, h_2$  and  $L_{12}$ . We can see from Fig. 8 (b) that the additional optimization over  $r_1$  shifts the channel of maximum radiation from  $l = 7$  to  $l = 9$  and increases the  $Q$ -factor by six times. One can speculate that the introduction of an additional parameter to vary could suppress more contributions into multipole radiation. For example, two dimers, as shown in Fig. 2 (b), provide more geometrical parameters than the previous case presented in Fig. 2 (a). The amplitudes of the multipole decomposition are shown in Fig. 9. We can see remarkable effect of destructive interference of complex multipole amplitudes  $a_{l0}$ . The left panels demonstrate the effect till  $l = 4$ , while the right panels do it till  $l = 14$ .

In subplots (c) and (d) the relative phases between amplitudes of both dimers are shown. One can observe in Fig. 9 almost full destructive interference of the multipolar amplitudes at the dominant channels  $l = 2, 4, 6$  from both dimers, when moduli of the coefficients are equal, while phases differ by  $\pi$ . The destructive interference of several amplitudes  $|a_{l0}|$  simultaneously was achieved owing to the multiscale optimization procedure only.

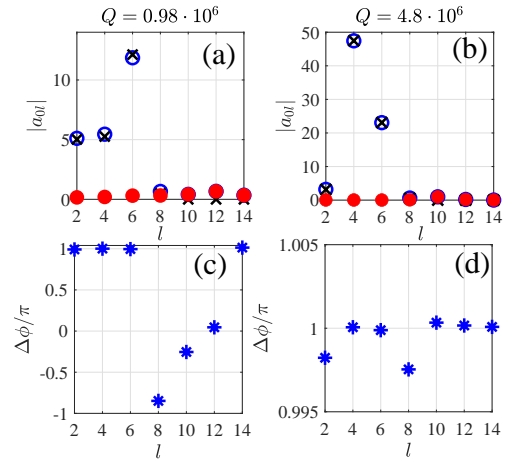


FIG. 9. The multipole radiation amplitudes  $a_{l0}, l = 2, 4, 6, \dots$  in Eq. (5) for the system of four disks with identical radii (mode 7 in Table I,  $Q = 9.8 \cdot 10^5$ ) (a) and (c). (b) and (d) is amplitudes  $a_{l0}$  for the system of four disks with different radii (mode 8 in Table I,  $Q = 4.8 \cdot 10^6$ ). The amplitudes of inner/outer dimer of disks are marked by crosses/open circles and amplitudes of the total system are marked by red closed circles.

## V. MODE VOLUMES OF RESONANCES WITH EXTREMAL $Q$ -FACTOR

Optical cavities are able to trap light at discrete resonant frequencies in a tiny volume in which the interaction of light with matter can be dramatically enhanced via temporal and spatial confinement of light. It is important not only to enhance the  $Q$ -factor. Miniaturization of cavities with a high  $Q/V_m$ -ratio is in demand to improve the light-matter interaction and reduce layout for compact integrated optical circuits.

The  $Q$ -factor and effective mode volume  $V_m$  – two figures of merit of optical cavities – are of great importance in the enhancement of light-matter interaction. The mode volume of a dielectric cavity is given by the ratio of the total electric energy to the maximum electric energy density<sup>63</sup>

$$V_m = \frac{\int \epsilon(\mathbf{x}) |\mathbf{E}(\mathbf{x})|^2 dV}{\max[\epsilon(\mathbf{x}) |\mathbf{E}(\mathbf{x})|^2]}. \quad (6)$$

A summary of the  $Q$ -factors and mode volumes are collected by Vahala<sup>4</sup> and range from  $Q = 2 \cdot 10^3$ ,  $V_m = 5(\lambda)^3$  (FPR),  $Q = 1.2 \cdot 10^4$ ,  $V_m = 6(\lambda)^3$  (WGM) till  $Q = 1.3 \cdot 10^4$ ,  $V_m = 1.2(\lambda)^3$  (PhC cavity). Ultra-low mode volumes in one-dimensional slotted photonic crystal single silicon nanobeam cavities of order  $(0.1 - 0.01)(\lambda/n)^3$  ( $n$  is refractive index of DS) were reported<sup>5-7</sup>, however, at the cost of compactness of resonator.

These data in Table are compared with whispering gallery mode with azimuthal number  $m = 10$  and the eigenfrequency  $\text{Re}(kr) = 4.76$  in single disk of aspect ratio  $h_1/r = 0.2588$ .

## VI. CONCLUSION AND OUTLOOK

The avoided crossing of resonances leads to substantial redistribution of their imaginary parts and hybridization of resonant modes<sup>32</sup>. This way of the  $Q$ -factor enhancement was turned out to be successful even in a single cavity shaped as disk<sup>39</sup> or long rod of rectangular cross-section<sup>37</sup>. The ACRs in two identical cavities lifts the  $Q$ -factor essentially more<sup>35,45,55,64</sup>. It might be seemed, a further increasing of the number  $N$  of identical cavities is the best way to enhance  $Q$ -factor because periodical array of cavities supports quasi-BICs<sup>24</sup> with asymptotic  $Q \sim N^2$ . However, this method of enhancement of  $Q$ -factor is bumping into saturation owing to material losses<sup>24</sup> and structural fluctuations<sup>65</sup>. Moreover, BIC modes concede in compactness of DS and mode volume. In the present paper we show that DS composed of cavities with different scales provides considerably larger  $Q$ -factors preserving the mode volume as Table I shows. And what is remarkable, this unprecedented values of the  $Q$ -factor refer to the compact DSs as crucially different from the extended periodical DSs supporting the quasi-BICs. The compactness of DS has a large technological advantage for sensing and lasing devices.

There is a useful tool to understand the nature of the extremely high quality factor for the avoided crossing through multipole decomposition<sup>56</sup>. That tool shed light on the origin

of the high  $Q$ -factor in the isolated disk<sup>41,57</sup> and the origin of bound states in the continuum<sup>58</sup>. In the present case of several cavities we also observe that extreme  $Q$ -factor is attributed to strong redistribution of radiation that originates from compensation of dominating multipole coefficients. Moreover, we show that it is related to almost perfect destructive interference of the low order multipole radiations from the inner subsystem inserted into the outer dimer.

Thus, the way to boost quality factor of the array of resonators looks simple. First, we attain the maximal  $Q$ -factor by ACRs in the inner subsystem of  $N - 2$  disks that results in some hybridized resonant mode  $\psi_{s,a}(N - 2)$ , which can be symmetric or antisymmetric relative to axis inversion. Then, we symmetrically enclose the inner subsystem into a shell consisted of two identical disks, which form an outer dimer. Varying the scales of dimer (radius  $r_1$ , height  $h_1$  and distance  $L_{12}$ ) we perform ACRs of resonant modes  $\psi_{s,a}(N - 2)$  with the resonant modes  $\psi_{s,a}(2)$  of the outer dimer. To achieve an extremal  $Q$ -factors one has to allow slight change of scales of inner subsystem too as it was shown in the Section III. Because of this, the optimization procedure should be performed over all scales of the total system. As a result, we can achieve almost perfect shielding of inner resonant mode by outer dimer and boost the  $Q$ -factor by several orders of magnitude. Some hybridized resonant modes are collected in Table I. Our results show that multiscale optimization procedure gives substantially higher results for the  $Q$ -factor compared to the case of equidistant identical disks, which supports quasi-BICs at  $\Gamma$ -point.

The proposed algorithm could be easily adopted to multi cavity systems of different shape and permittivity. The present system of coaxial disks was chosen because of separation of polarizations in the sector of zero azimuthal index. It should be noted that the  $Q$ -factor of optimized systems is very sensitive to scale parameters however. Especially to parameters, which affect the resonant mode  $\psi_{N-2}$  of the inner subsystem because of weak localization of the total mode  $\psi_N$  at outside dimer. This brings definite technological problems because of necessity to accurately set up different scales of different resonators. Fortunately, S. Kim *et al*<sup>66</sup> reported control over disk dimensions with accuracy 5 nm in optical range, i.e., 0.3 percent relative to the optical wave length  $\lambda = 1.55 \mu\text{m}$ .

**Acknowledgement:** We acknowledge discussions with Yi Xu.

**Funding:** This work is supported by the Russian Science Foundation under grant 22-12-00070.

**Conflict of interest statement:** The authors declare no conflicts of interest regarding this article.

<sup>1</sup>G. Mie, "Beiträge zur optik trüber medien, speziell kolloidaler metallösungen," *Annalen der Physik* **330**, 377–445 (1908).

<sup>2</sup>D. Colton and R. Kress, *Inverse Acoustic and Electromagnetic Scattering Theory*, 2nd ed. (Springer, Berlin, 1998).

<sup>3</sup>M. G. Silveirinha, "Trapping light in open plasmonic nanostructures," *Phys. Rev. A* **89**, 023813 (2014).

<sup>4</sup>K. Vahala, "Optical microcavities," *Nature* **424**, 839–846 (2003).

<sup>5</sup>J. Ryckman and S. M. Weiss, "Low mode volume slotted photonic crystal single nanobeam cavity," *Appl. Phys. Lett.* **101**, 071104 (2012).

<sup>6</sup>P. Seidler, K. Lister, U. Drechsler, J. Hofrichter, and T. Stöferle, "Slotted photonic crystal nanobeam cavity with an ultrahigh quality factor-to-mode volume ratio," *Optics Express* **21**, 32468 (2013).

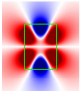
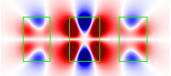
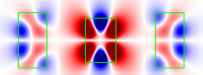
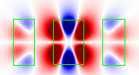
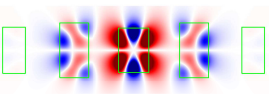
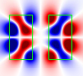
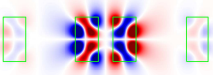
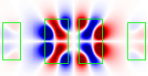
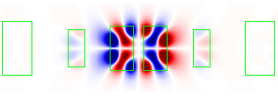
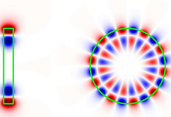
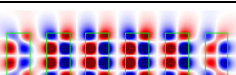
	Mode profile $\text{Re}(E_\phi)$	Scales	$\text{Re}(kr)$	$Q$	$V_m \left(\frac{n}{\lambda}\right)^3$
1		$h_1/r = 1.4157$	1.72	$1.5 \cdot 10^2$	1.4
2		$h_1/r = 1.257, r_1/r = 1$ $h_2/r = 1.362, L_{12}/r = 0.873$	1.76	$9.8 \cdot 10^3$	1.6
3		$h_1/r = 1.292, r_1/r = 1.243$ $h_2/r = 1.375, L_{12}/r = 1.78$	1.75	$5.8 \cdot 10^4$	1.6
4		$h_1/r = 0.9972, r_1/r = 1.0363$ $h_2/r = 1.3709, L_{12}/r = 0.8497$	1.76	$6.6 \cdot 10^4$	1.4
5		$h_1/r = 1.0237, r_1/r = 1.0398$ $h_2/r = 1.3025, r_2/r = 1.2319$ $h_3/r = 1.3629, L_{12}/r = 1.5468$ $L_{23}/r = 1.3879$	1.77	$8.5 \cdot 10^7$	1.7
6		$h_1/r = 1.038, L_{12}/r = 0.734$	2.19	$5.7 \cdot 10^3$	1.9
7		$h_1/r = 1.0173, r_1/r = 1$ $h_2/r = 1.039, L_{12}/r = 2.2731$ $L_{23}/r = 0.6585$	2.19	$9.8 \cdot 10^5$	2
8		$h_1/r = 0.7988, r_1/r = 0.8368$ $h_2/r = 1.0503, L_{12}/r = 1.1424$ $L_{23}/r = 0.4922$	2.2	$4.8 \cdot 10^6$	2.1
9		$h_1/r = 1.3257, r_1/r = 1.2136$ $h_2/r = 0.7479, r_2/r = 0.8376$ $h_3/r = 1.05326, L_{12}/r = 1.6345$ $L_{23}/r = 1.1869, L_{34}/r = 0.46103$	2.2	$1.3 \cdot 10^9$	2.1
10		$h_1/r = 0.2588, m = 10$	4.76	$6 \cdot 10^6$	4.9
11		$h_1 = h_2 = h_3 = 1.038r$ $r_1 = r_2 = r$ $L_{12} = L_{23} = L_{34} = 0.734r$	2.19	$2.4 \cdot 10^3$	4.4

TABLE I. Mode profiles and parameters of optimized systems of several coaxial disks.

- <sup>7</sup>J. Zhou, J. Zheng, Z. Fang, P. Xu, and A. Majumdar, "Ultra-low mode volume on substrate silicon nanobeam cavity," *Optics Express* **27**, 30692 (2019).
- <sup>8</sup>V. Braginsky, M. Gorodetsky, and V. Ilchenko, "Quality-factor and nonlinear properties of optical whispering-gallery modes," *Phys. Let. A* **137**, 393 (1989).
- <sup>9</sup>M. Gorodetsky and A. Fomin, "Geometrical theory of whispering-gallery modes," *IEEE J. Selected Topics in Quantum Electronics* **12**, 33–39 (2006).
- <sup>10</sup>N. Acharyya and G. Kozyreff, "Large q factor with very small whispering gallery mode resonators," *Phys. Rev. Appl.* **12**, 014060 (2019).
- <sup>11</sup>X. Jiang, A. Qavi, S. Huang, and L. Yang, "Whispering-gallery sensors," *Matter* **3**, 371–392 (2020).
- <sup>12</sup>S. H. Hong, Y. J. Lee, S. Hong, Y. Kim, and S.-H. Kwon, "An-

- isymmetric mode cancellation for high-Q cavities in a double disk," *Photonics* **9**, 572 (2022).
- <sup>13</sup>Chia Wei Hsu, Bo Zhen, A. D. Stone, J. D. Joannopoulos, and M. Soljačić, "Bound states in the continuum," *Nature Reviews Materials* **1**, 16048 (2016).
- <sup>14</sup>S. Azzam and A. Kildishev, "Photonic bound states in the continuum: From basics to applications," *Adv. Opt. Mat.* **9**, 2001469 (2020).
- <sup>15</sup>L. Huang, L. Xu, M. Woolley, and A. E. Miroshnichenko, "Trends in quantum nanophotonics," *Advanced Quantum Technologies* **3**, 1900126 (2020).
- <sup>16</sup>S. Joseph, S. Pandey, S. Sarkar, and J. Joseph, "Bound states in the continuum in resonant nanostructures: an overview of engineered materials for tailored applications," *Nanophotonics* **10**, 4175–4207 (2021).
- <sup>17</sup>K. Koshelev, Z. Sadrieva, A. Shcherbakov, Y. Kivshar, and A. Bogdanov, "Bound states in the continuum in photonic structures,"

- Uspekhi Fizicheskikh Nauk **65**, 039120 (2022), 2207.01441v2.
- <sup>18</sup>P. Hu, C. Xie, Q. Song, A. Chen, H. Xiang, D. Han, and J. Zi, "Bound states in the continuum based on the total internal reflection of bloch waves," *Nat. Sci. Review* (2022), 10.1093/nsr/nwac043.
  - <sup>19</sup>Chia Wei Hsu, Bo Zhen, Jeongwon Lee, S. G. Johnson, J. D. Joannopoulos, and M. Soljačić, "Observation of trapped light within the radiation continuum," *Nature* **499**, 188 (2013).
  - <sup>20</sup>E. Bulgakov and A. Sadreev, "Bound states in the continuum with high orbital angular momentum in a dielectric rod with periodically modulated permittivity," *Phys. Rev. A* **96**, 013841 (2017).
  - <sup>21</sup>K. Koshelev, G. Favraud, A. Bogdanov, Y. Kivshar, and A. Fratalocchi, "Nonradiating photonics with resonant dielectric nanostructures," *Nanophotonics* **8**, 725 (2019).
  - <sup>22</sup>A. Taghizadeh and I.-S. Chung, "Quasi bound states in the continuum with few unit cells of photonic crystal slab," *Appl. Phys. Lett.* **111**, 031114 (2017).
  - <sup>23</sup>E. Bulgakov and A. Sadreev, "Propagating bloch bound states with orbital angular momentum above the light line in the array of dielectric spheres," *J. Opt. Soc. Am. A* **34**, 949 (2017).
  - <sup>24</sup>Z. F. Sadrieva, M. A. Belyakov, M. A. Balezin, P. V. Kapitanova, E. A. Nenasheva, A. F. Sadreev, and A. A. Bogdanov, "Experimental observation of a symmetry-protected bound state in the continuum in a chain of dielectric disks," *Phys. Rev. A* **99**, 053804 (2019).
  - <sup>25</sup>I. Y. Polishchuk, A. A. Anastasiev, E. A. Tsyvkunova, M. I. Gozman, S. V. Solov'ov, and Y. I. Polishchuk, "Guided modes in the plane array of optical waveguides," *Phys. Rev. A* **95**, 053847 (2017).
  - <sup>26</sup>M. Sidorenko, O. Sergaeva, Z. Sadrieva, C. Roques-Carmes, P. Mu-raev, D. Maksimov, and A. Bogdanov, "Observation of an accidental bound state in the continuum in a chain of dielectric disks," *Phys. Rev. Appl.* **15**, 034041 (2021).
  - <sup>27</sup>E. Bulgakov and A. Sadreev, "High-Q resonant modes in a finite array of dielectric particles," *Phys. Rev. A* **99**, 033851 (2019).
  - <sup>28</sup>E. Bulgakov and D. Maksimov, "Q -factor optimization in dielectric oligomers," *Phys. Rev. A* **100**, 033830 (2019).
  - <sup>29</sup>D. F. Kornovan, R. S. Savelev, Y. Kivshar, and M. I. Petrov, "High-Q localized states in finite arrays of subwavelength resonators," *ACS Photonics* **8**, 3627–3632 (2021).
  - <sup>30</sup>Y. Gao and Y. Shi, "Design of a single nanoparticle trapping device based on bow-tie-shaped photonic crystal nanobeam cavities," *IEEE Photonics Journal* **11**, 1–8 (2019).
  - <sup>31</sup>P. von Brentano, "On the generalization of the level repulsion theorem to resonances," *Phys. Lett. B* **238**, 1 (1990).
  - <sup>32</sup>W. D. Heiss, "Repulsion of resonance states and exceptional points," *Phys. Rev. E* **61**, 929–932 (2000).
  - <sup>33</sup>H. Cao and J. Wiersig, "Dielectric microcavities: Model systems for wave chaos and non-hermitian physics," *Rev. Mod. Phys.* **87**, 61 (2015).
  - <sup>34</sup>N. R. Bernier, L. D. Tóth, A. K. Feofanov, and T. J. Kippenberg, "Level attraction in a microwave optomechanical circuit," *Phys. Rev. A* **98**, 023841 (2018).
  - <sup>35</sup>J. Wiersig, "Formation of Long-Lived, Scarlike Modes near Avoided Resonance Crossings in Optical Microcavities," *Phys. Rev. Lett.* **97**, 253901 (2006).
  - <sup>36</sup>Y. Yang, A. Miroshnichenko, S. Kostinski, M. Odit, P. Kapitanova, M. Qiu, and Y. Kivshar, "Multimode directionality in all-dielectric metasurfaces," *Phys. Rev. B* **95**, 165426 (2017).
  - <sup>37</sup>L. Huang, L. Xu, M. Rahmani, D. Neshev, and A. Miroshnichenko, "Pushing the limit of high-Q mode of a single dielectric nanocavity," *Advanced Photonics* **3**, 016004 (2021).
  - <sup>38</sup>Q. H. Song and H. Cao, "Improving optical confinement in nanostructures via external mode coupling," *Phys. Rev. Lett.* **105**, 053902 (2010).
  - <sup>39</sup>M. Rybin, K. Koshelev, Z. Sadrieva, K. Samusev, A. Bogdanov, M. Limonov, and Y. Kivshar, "High-Q Supercavity Modes in Subwavelength Dielectric Resonators," *Phys. Rev. Lett.* **119**, 243901 (2017).
  - <sup>40</sup>K. Koshelev, A. Bogdanov, and Y. Kivshar, "Meta-optics and bound states in the continuum," *Science Bulletin* **17**, 065601 (2018).
  - <sup>41</sup>W. Chen, Y. Chen, and W. Liu, "Multipolar conversion induced subwavelength high-q kerker supermodes with unidirectional radiations," *Laser & Photonics Reviews* **13**, 1900067 (2019).
  - <sup>42</sup>W. Wang, L. Zheng, L. Xiong, J. Qi, and B. Li, "High Q-factor multiple fano resonances for high-sensitivity sensing in all-dielectric metamaterials," *OSA Continuum* **2**, 2818 (2019).
  - <sup>43</sup>M. Odit, K. Koshelev, S. Gladyshev, K. Ladutenko, Y. Kivshar, and A. Bogdanov, "Observation of supercavity modes in subwavelength dielectric resonators," *Advanced Materials*, 2003804 (2020).
  - <sup>44</sup>I. Volkovskaya, L. Xu, L. Huang, A. Smirnov, A. Miroshnichenko, and D. Smirnova, "Multipolar second-harmonic generation from high-q quasi-BIC states in subwavelength resonators," *Nanophotonics* **9**, 3953 (2020).
  - <sup>45</sup>S. V. Boriskina, "Theoretical prediction of a dramatic q-factor enhancement and degeneracy removal of whispering gallery modes in symmetrical photonic molecules," *Opt. Lett.* **31**, 338 (2006).
  - <sup>46</sup>S. Boriskina, "Coupling of whispering-gallery modes in size-mismatched microdisk photonic molecules," *Opt. Lett.* **32**, 1557 (2007).
  - <sup>47</sup>M. Benyoucef, J.-B. Shim, J. Wiersig, and O. G. Schmidt, "Quality-factor enhancement of supermodes in coupled microdisks," *Opt. Lett.* **36**, 1317 (2011).
  - <sup>48</sup>S.-H. G. Chang and C.-Y. Sun, "Avoided resonance crossing and non-reciprocal nearly perfect absorption in plasmonic nanodisks with near-field and far-field couplings," *Optics Express* **24**, 16822 (2016).
  - <sup>49</sup>K. N. Pichugin and A. F. Sadreev, "Interaction between coaxial dielectric disks enhances the Q factor," *J. Appl. Phys.* **126**, 093105 (2019).
  - <sup>50</sup>E. N. Bulgakov, K. N. Pichugin, and A. F. Sadreev, "Evolution of the resonances of two parallel dielectric cylinders with distance between them," *Phys. Rev. A* **100**, 043806 (2019).
  - <sup>51</sup>A. Dmitriev and M. Rybin, "Combining isolated scatterers into a dimer by strong optical coupling," *Phys. Rev. A* **99**, 063837 (2019).
  - <sup>52</sup>V. Vinel, Z. Li, A. Borne, A. Bensemhoun, I. Favero, C. Ciuti, and G. Leo, "Non-hermitian bath model for arrays of coupled nanoresonators," *Optics Express* **29**, 34015 (2021).
  - <sup>53</sup>K. Pichugin, A. Sadreev, and E. Bulgakov, "Ultrahigh-Q system of a few coaxial disks," *Nanophotonics* **10**, 4341–4346 (2021).
  - <sup>54</sup>R. Kitamura, L. Pilon, and M. Jonasz, "Optical constants of silica glass from extreme ultraviolet to far infrared at near room temperature," *Appl. Optics* **46**, 8118 (2007).
  - <sup>55</sup>E. Bulgakov, K. Pichugin, and A. Sadreev, "Mie resonance engineering in two disks," *MDPI Photonics* **8**, 49 (2021).
  - <sup>56</sup>J. D. Jackson, *Classical Electrodynamics* (John Wiley and Sons, Inc., New York, 1962).
  - <sup>57</sup>A. Bogdanov, K. Koshelev, P. Kapitanova, M. Rybin, S. Gladyshev, Z. Sadrieva, K. Samusev, Y. Kivshar, and M. F. Limonov, "Bound states in the continuum and Fano resonances in the strong mode coupling regime," *Adv. Photonics* **1**, 1 (2019).
  - <sup>58</sup>Z. Sadrieva, K. Frizyuk, M. Petrov, Y. Kivshar, and A. Bogdanov, "Multipolar origin of bound states in the continuum," *Phys. Rev. B* **100** (2019), 10.1103/physrevb.100.115303.
  - <sup>59</sup>J. A. Stratton, *Electromagnetic theory*, edited by L. A. DuBridge (McGraw-Hill Book Company, Inc., 1941).
  - <sup>60</sup>C. Linton, V. Zalipae, and I. Thompson, "Electromagnetic guided waves on linear arrays of spheres," *Wave Motion* **50**, 29–40 (2013).
  - <sup>61</sup>E. Bulgakov, K. Pichugin, and A. Sadreev, "Exceptional points in a dielectric spheroid," *Phys. Rev. A* **104**, 053507 (2021).
  - <sup>62</sup>A. Doicu, T. Wriedt, and Y. A. Eremin, *Light Scattering by Systems of Particles* (Springer Berlin Heidelberg, 2006).
  - <sup>63</sup>S. Hu and S. Weiss, "Design of photonic crystal cavities for extreme light concentration," *ACS Photonics* **3**, 1647 (2016).
  - <sup>64</sup>F. Vennberg, A. Ravishankar, and S. Anand, "Manipulating light scattering and optical confinement in vertically stacked Mie resonators," *Nanophotonics* **11**, 4755 (2022).
  - <sup>65</sup>E. Maslova, M. Rybin, A. Bogdanov, and Z. Sadrieva, "Bound states in the continuum in periodic structures with structural disorder," *Nanophotonics* **10**, 4313–4321 (2021).
  - <sup>66</sup>S. Kim, K.-H. Kim, and J. Cahoon, "Optical bound states in the continuum with nanowire geometric superlattices," *Phys. Rev. Lett.* **122**, 187402 (2019).